京都大学学術情報リポジトリ
KURENAI 紅
Kyoto University Research Information Repository

京都大学
KYOTO UNIVERSITY

RESEARCH ARTICLE

Solar

Bilayer Indium Tin Oxide Electrodes for Deformation-Free Ultrathin Flexible Perovskite Solar Cells

Noboru Ohashi,* Ryuji Kaneko, Chikako Sakai, Yoko Wasai, Seiji Higuchi, Kenji Yazawa, Hirokazu Tahara, Taketo Handa, Tomoya Nakamura, Richard Murdey, Yoshihiko Kanemitsu, and Atsushi Wakamiya*

The superior electrical conductivity and optical transparency of indium tin oxide (ITO) make it an ideal electrode material for use in optoelectronic devices such as solar cells. When ITO electrodes are fabricated on very thin plastic substrates, however, the internal stress of the ITO layer causes the substrate to deform, severely limiting the device's performance. Herein, it is shown that ITO bilayers composed of an amorphous base layer and a crystalline overlayer lead to deformation-free ITO electrodes. It is shown that an optimized bilayer structure is achieved when the internal stresses of the amorphous and crystalline layers approximately cancel. With this approach, mixed composition metal halide perovskite solar cells with ITO electrodes are successfully fabricated on 4 µm polyethylene naphthalate films. A power conversion efficiency (PCE) of 18.2% is obtained for the reference cell design, corresponding to a power-to-weight ratio of 24 W g^{-1} before encapsulation. The devices retain 95% of the original PCE after 1000 bend cycles, while under simulated indoor lighting (white LED, 200 lux, 5000 K) the PCE reaches 28.3%. A 3-cell module with a designated area of 2.3 cm^2 is realized with a power output of 28.1 mW and an open-circuit voltage of 3.17 V.

1. Introduction

Metal halide perovskites are attractive absorber materials for efficient solar cells.[1] The power conversion efficiency (PCE) of single-junction perovskite solar cells now exceeds 25% while the PCE of crystalline silicon/perovskite tandem solar cells has reached over 30%.[2–4] Recently, research efforts have focused on developing ultralight solar cells for portable/mobile electronics applications such as wearable devices, robotics, and lightweight drones.[5–9] As the active layers in thin film electronic devices are typically less than 1 µm thick, the weight of the device before encapsulation is largely defined by the substrate. Therefore, the main challenge for realizing lightweight, flexible devices with high power-to-weight ratios is how to reduce the substrate thickness without compromising device performance.

Polyethylene terephthalate (PET) or polyethylene naphthalate (PEN) films coated with a thin layer of transparent conductive oxide (TCO)—typically indium tin oxide (ITO)—are frequently used as the substrate for thin film devices.[6] These films, which are typically 100 µm thick, retain a usefully high stiffness making them relatively easy to process. In order to maximize the power-to-weight ratio, however, even thinner substrates are desirable. For example, extremely lightweight solar cells with power-to-weight ratios of over 20 W g^{-1} could be realized if the substrate thickness is reduced to less than 10 µm.[10–14] As a point of reference, this is two orders of magnitude higher than the conventional crystalline Si cells before encapsulation/packaging is considered.[15] However, fabricating solar cells on these ultrathin substrates is difficult due to their overall fragility, poor thermal stability, and lack of mechanical rigidity. As a result, many otherwise promising solar cell technologies are incompatible with these ultrathin plastic substrates. Among silicon, organic heterojunction, and metal halide perovskite solar cells, perovskite devices stand out for their unique combination of high performance, low cost, and ease of processing.[16]

In solar cells, the front-facing electrode must combine good optical transparency with high electrical conductivity. An excellent choice for this application is ITO, a transparent, conductive, and durable material, that can be readily prepared in industrial

N. Ohashi, R. Kaneko, C. Sakai, K. Yazawa, H. Tahara, T. Handa,
T. Nakamura, R. Murdey, Y. Kanemitsu, A. Wakamiya
Institute for Chemical Research
Kyoto University
Uji, Kyoto 611-0011, Japan
E-mail: ohashi.noboru.6n@kyoto-u.ac.jp; wakamiya@scl.kyoto-u.ac.jp

Y. Wasai
Analytical Technology Department
HORIBA Techno Service Co., Ltd.
Chiyoda-ku, Tokyo 101-0063, Japan

S. Higuchi
Scientific/Semiconductor Product R&D Center
HORIBA, Ltd.
Minami-ku, Kyoto 601-8510, Japan

京都大学
KYOTO UNIVERSITY

**ADVANCED
SCIENCE NEWS**

www.advancedsciencenews.com

京都大学学術情報リポジトリ
KURENAI 紅
Kyoto University Research Information Repository

Solar

www.solar-rrl.com

quantities. However, when working with ultrathin plastic substrates less than 10 µm, poly(3,4-ethylenedioxythiophene):polystyrene sulfonate (PEDOT:PSS) is often used instead of ITO, despite its lower conductivity and limited long-term stability.[15,17] This is most likely due to the difficulties encountered when attempting to fabricate ITO films on ultrathin plastic substrates. Indeed, we confirmed that ultrathin plastic substrates deform when ITO layers are deposited by conventional magnetron sputtering and that this resulted in very poor solar cell performance.

In the present work, which has been ongoing for several years,[18] we show that deformation-free ITO-coated 4 µm PEN substrates can be obtained by sequentially growing amorphous and crystalline ITO layers in a bilayer structure combining different thicknesses of amorphous and crystalline ITO layers chosen to minimize the internal stress. The bilayer films are confirmed to have high transparency and good electrical conductivity. The utility of stress compensation was recently confirmed by U. Kim et al., who were able to reduce internal stress in PEN/ITO films by applying a layer of AlO_x to the opposite surface of the PEN film.[19]

Our deformation-free, optimized bilayer ITO enabled the fabrication of high-performance ultrathin, flexible perovskite solar cells and modules: Under AM1.5G simulated solar irradiation the maximum PCE of the solar cells was 18.2% while the power-to-weight ratio of the solar cells reached 24 W g^{-1}. High efficiency was retained under ambient light, an important consideration for internet-of-things applications: The PCE, when operated under a white LED (5000 K) at 200 lx, reached 28.3%. Picosecond laser scribing (532 nm and 0.1–0.3 W) enabled the fabrication of 3-cell modules with a designated area of 2.3 cm^2 on fragile ultrathin PEN films. The maximum power output of the module under AM1.5G was 28.1 mW, with a V_{oc} of 3.17 V—exceeding 1 V cell^{-1} and sufficient to power a small LED.

2. Results and Discussion

2.1. ITO Layers Characterization

Highly crystalline ITO layers are desirable for electronic device applications as they generally have the highest electrical conductivity and optical transparency.[20] When growing ITO films by sputter deposition, high crystallinity can be assured by maintaining the substrate at an elevated temperature. ITO layers with good crystallinity (ITO-C) could be readily fabricated by increasing the substrate temperature to 150 °C and reducing the chamber pressure to 0.1 Pa.[21,22] As the temperature of the plastic substrates cannot exceed 150 °C, a relatively low chamber pressure was needed to achieve suitably high crystallinity. As a result of sputtering at such low pressure, however, the ITO films develop high negative internal stress, a phenomenon known as the peening effect.[23,24] In contrast, amorphous ITO (ITO-A), which could be prepared by sputtering at room temperature with a chamber pressure of 5 Pa, is known to have positive internal stress.[25] Confirmation of the crystallinity and morphology of the crystalline and amorphous ITO layers on glass substrates is given in Figure S1, Supporting Information.

As illustrated in **Figure 1**a, based on a simple geometric model we can anticipate minimal deformation of the ultrathin film substrates when the sum of the positive and negative internal stresses in the ITO-A/ITO-C bilayer is close to zero. As the internal stress is proportional to the film thickness, the opposing forces in the bilayer can be balanced out by simply varying the thickness ratio of the ITO-A and ITO-C layers. In addition to internal stress, however, other properties of the bilayer film relevant to its function as the transparent electrode such as optical transparency and electrical conductivity must also be taken into consideration. Most importantly, ITO-A is not an effective electrode material due to its poor conductivity. ITO-C should be as thick as possible to minimize resistive losses, while the overall thickness of the bilayer should be as thin as possible to maximize optical transparency.

The internal stress of a coating film, σ_f, can be estimated from the radius of substrate curvature using Stoney's equation[26,27]

$$\sigma_f = \frac{E_s t_s^2}{6(1-\nu_c)t_f R} \tag{1}$$

where E_s is Young's modulus of the substrate, t_s is the thickness of the substrate, ν_c is Poisson's ratio of the substrate, R is the
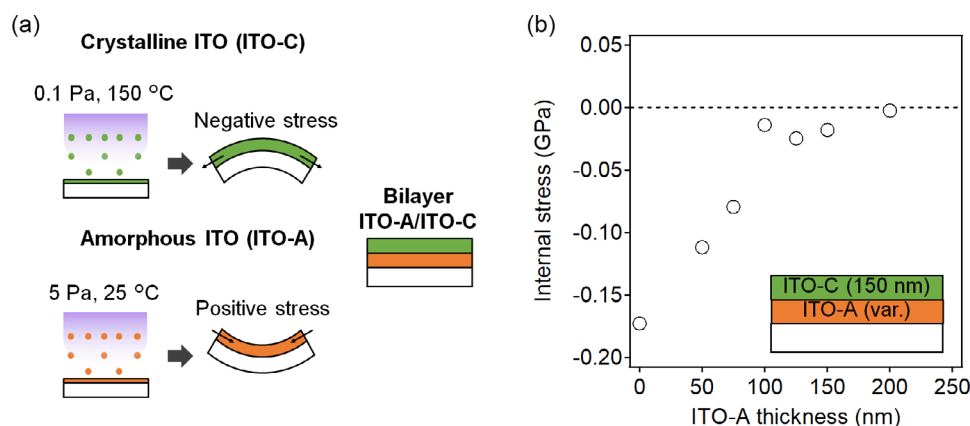

Figure 1. A method for fabricating deformation-free indium tin oxide electrodes on ultrathin films. a) Schematic illustration of the effects of positive and negative internal stress in sputtered ITO layers. b) Variation in internal stress as the thickness of the ITO-A layer is increased, for a constant ITO-C overlayer thickness of 150 nm.

radius of curvature of the substrate, and t_f is the film thickness (see Figure S2, Supporting Information, for details). The model is valid for $t_f << t_s$, a condition that is not fulfilled for ITO layers on ultrathin PEN. The internal stress of the ITO on ultrathin PEN was therefore estimated from values obtained for ITO layers deposited on 50 µm-thick glass substrates. The curvature of the glass substrate was measured before and after the deposition of the ITO layers, and the difference in curvature was used as the value of R to calculate the internal stress using Equation (1). Equation (1) only approximates the internal stress if the thermal stress due to the differential coefficient of thermal expansion (CTE) of the substrate and ITO is sufficiently small to be considered negligible.[28,29] Fortunately, the CTE of PEN ($1.03 \times 10^{-5}\,K^{-1}$), cover glass ($0.72 \times 10^{-5}\,K^{-1}$), and ITO ($\approx 1.02 \times 10^{-5}\,K^{-1}$) are similar.[30–33] The contributions from thermal stress are therefore expected to be small for both the PEN/ITO and glass/ITO systems. The crystallinity, film morphology, and optical properties of the ITO films deposited on PEN substrates (Figure S3, Supporting Information) are broadly similar to those of ITO deposited on glass (see Figure S1 and S4, Supporting Information). Therefore, we feel it is reasonable to assume that the stress characteristics of the sputtered ITO layers are primarily determined by the deposition parameters and are largely independent of the substrate. Amorphous ITO layers induced concave curvature in the glass substrates, while convex curvature was induced in the glass substrates when crystalline ITO layers were deposited (see Figure S5, Supporting Information). The internal stress of 150 nm-thick single ITO-A and ITO-C layers was found to be +0.033 and −0.17 GPa, respectively. Note that the conductivity of ITO-A at 67 S cm^{-1} was confirmed to be much lower than the ITO-C layer, which was estimated at 2100 S cm^{-1}. Parameters of ITO-A and ITO-C layers are given in Table S1, Supporting Information. While the conductivity of the ITO-C layer is lower than commercially available glass/ITO (≈ 5000 S cm^{-1}) as a result of the temperature limitations imposed on the sputtering process, it still exceeds that of high conductivity PEDOT:PSS (≈ 1000 S cm^{-1}).[34] In principle, we would therefore expect ITO-C to perform better than PEDOT:PSS in device applications.

To determine how the balance of internal stress varied with film thickness, the thickness of ITO-C was fixed at 150 nm (the minimum thickness needed to maintain usefully high electrical conductivity), while the thickness of the ITO-A underlayer was varied from 0 to 200 nm. As shown in Figure 1b, the internal stress decreased linearly as the ITO-A layer thickness was increased, and approached zero at 200 nm. These measurements reveal that the internal stress of the ITO bilayer can be significantly modified by the thickness of ITO-A layers up to 125 nm.

The optical transmittance spectra of the ITO bilayers are shown in **Figure 2**. The region from 400 to 800 nm for which the average transmittance is calculated approximates the range of optical active wavelengths of typical perovskite solar cells. While the transparency of the ITO films varied due to optical interference effects, it is nevertheless clearly desirable to limit the total thickness to 200 nm or less to maximize transparency. On the other hand, the thickness of the ITO-A layers should ideally be greater than 100 nm or more to fully mitigate the internal stress. Finally, the thickness of ITO-C should be maximized to increase the electrical conductance. These conflicting requirements make it
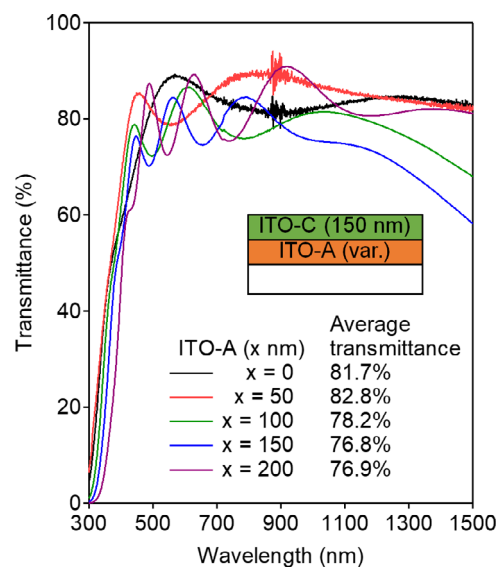

Figure 2. The optical transmittance spectra of ITO-A/ITO-C bilayers on glass. The thickness of the ITO-C overlayer is fixed at 150 nm, while the thickness of the ITO-A layer is varied between 0 and 200 nm. The average transmittance between 400 and 800 nm is indicated for each bilayer.

difficult to predict the best combination of film thickness for practical use. We therefore further refined the parameter space around the nominal center values by varying the thickness of the ITO-C layer slightly and adjusting the thickness of the ITO-A to keep the total bilayer thickness constant at 200 nm. In **Table 1**, the internal stress, optical transmittance, and layer conductivity are compared for three ITO-A/ITO-C bilayers: 50/150, 75/125, and 100/100 nm. As ITO-C is replaced with ITO-A in these bilayers, the internal stress decreases at the expense of lower conductivity. As the optical transparency for all three 200 nm bilayers remains above 82%, all three were deemed potentially viable configurations. Therefore, solar cell devices were prepared to evaluate the performance of each bilayer directly.

Ultrathin film substrates were prepared with the three optimized ITO bilayers in order to fabricate the perovskite solar cells for testing and evaluation. To realize this, 4 µm PEN films were mounted on rigid glass plates coated with an optically clear adhesive (OCA). ITO-A and ITO-C layers were deposited on the glass-backed PEN films using the sputter deposition parameters given in Table S1, Supporting Information. As shown in **Figure 3**, a 200 nm ITO-C layer grown directly on PEN causes

Table 1. Properties of three trial 200 nm ITO-A/ITO-C bilayer compositions on glass substrates.

Thickness (ITO-A) [nm]	Thickness (ITO-C) [nm]	Internal stress σ_f [GPa]	Average transmittance, $T_{avg.}$[a),b)] [%]	Sheet resistance, R [$\Omega\,sq^{-1}$]
50	150	−0.110	82.8	28
75	125	−0.056	82.2	33
100	100	+0.023	82.1	38

[a)]UV–vis spectra are given in Figure S3, Supporting Information. [b)]Average transmittance calculated for 400–800 nm bandwidth.
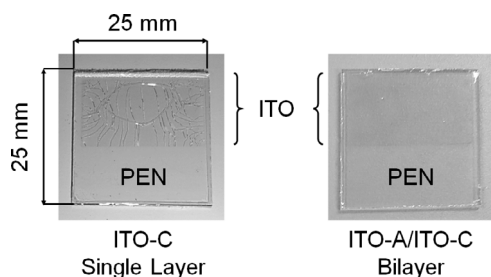
Figure 3. Photographs of a 200 nm ITO-C single layer (left) and 100/100 nm ITO-A/ITO-C bilayer (right) grown on 4 μm ultrathin PEN films, mounted on 25 mm × 25 mm glass substrates. The visible deformation of the 200 nm PEN/ITO-C system is avoided when the ITO-C layer is replaced by the stress-compensated ITO-A/ITO-C bilayer.

significant wrinkling of the film, and solar cells prepared on the wrinkled substrate were nonfunctional (see Figure S6, Supporting Information). In contrast, the PEN films with 50/150, 75/125, or 100/100 nm ITO-A/ITO-C bilayers remained smooth. When the total thickness of the ITO-A layer exceeded 50 nm, deformation-free films could be reliably prepared (see Figure S7, Supporting Information). We note that wrinkles were formed when the order in the bilayer was inverted and ITO-C was grown directly on the PEN (see Figure S8, Supporting Information). This is likely caused by the higher internal stress present in the ITO-C layer, which induced irreversible deformation in the PEN films before the compensating ITO-A layer could be applied.

2.2. Solar Cell Fabrication and Characterization

The deformation-free ITO layers were successfully applied to the fabrication of ultrathin perovskite solar cells. The n–i–p cell structure, illustrated in **Figure 4**a, is PEN (4000 nm)/ITO bilayer (200 nm)/SnO$_2$ (40 nm)/perovskite (500 nm)/Spiro-OMeTAD (200 nm)/Au (80 nm). The thickness of the entire functional solar cell is just over 5 μm. A triple cation perovskite, Cs$_{0.05}$FA$_{0.80}$MA$_{0.15}$PbI$_{2.65}$Br$_{0.35}$ (MA: methylammonium, FA: formamidinium) with a bandgap of 1.57 eV, was used as the active layer.[35]

The performance characteristics under AM1.5G for devices prepared with 50/150, 75/125, or 100/100 nm ITO-A/ITO-C bilayers are given in Figure 4b. For ease of handling, current–voltage (J–V) curves were measured with the devices still attached to the glass backing plates. Removing the devices from the backing plates did not materially influence the cell performance (see Figure S10, Supporting Information). The statistical variation of the device efficiencies is shown in Figure 4c. The maximum (median, interquartile range) PCE for the solar cells with 50/150, 75/125, and 100/100 nm ITO bilayers was 8.85% (5.60%, 2.14%), 16.8% (15.0%, 4.60%), and 11.4% (7.52%, 5.65%), respectively. Of the three ITO bilayers, the combination of 75 nm ITO-A with 125 nm ITO-C resulted in the best solar cell performance. Its combination of low stress, high transparency, and high conductivity is optimal for our device applications.

Next, the performance of the ultrathin perovskite solar cells with this 75/125 nm ITO-A/ITO-C bilayer was further refined by passivating the SnO$_2$ transport layers with halide ions (Cl$^-$ or F$^-$) in order to enhance the V_{oc} and to suppress the hysteresis of the J–V curves.[36–39] As shown in **Figure 5**a, after passivation of SnO$_2$, the PCE of the champion cell reached 18.2%, with J_{sc} of 22.0 mA cm^{-2}, V_{oc} of 1.09 V, and a fill factor (FF) of 0.76. The J–V curves have minimal hysteresis. 1000 s stabilized power output (SPO) curves measured under a nitrogen atmosphere are shown in Figure S11, Supporting Information. The output power remained above 99% after 1000 s. The median PCE was 15% and the statistical distribution of the PCE results is shown in Figure S12, Supporting Information. The stability of the devices was excellent, with the PCE of the devices remaining essentially unchanged even after 1 year of dark storage under N$_2$ atmosphere (shown in Figure S13, Supporting Information). The performance is superior to comparable reports obtained with PEDOT:PSS electrodes, largely due to the higher output voltages.[12,14,15] Without the glass backing plate, the weight per unit area is calculated to be 0.75 mg cm^{-2}. The power-to-weight ratio, determined using only the active area of the devices, is 24 W g^{-1}.

The external quantum efficiency shown in Figure 5b remained near 90% over most of the working spectral range of the cell, confirming the high transparency of the ITO layer. The integrated J_{sc} was 21.8 mA cm^{-1}, in good agreement with the J–V measurements. The strong attenuation in the UV region is from the absorption of the PEN substrate (see Figure S14, Supporting Information).
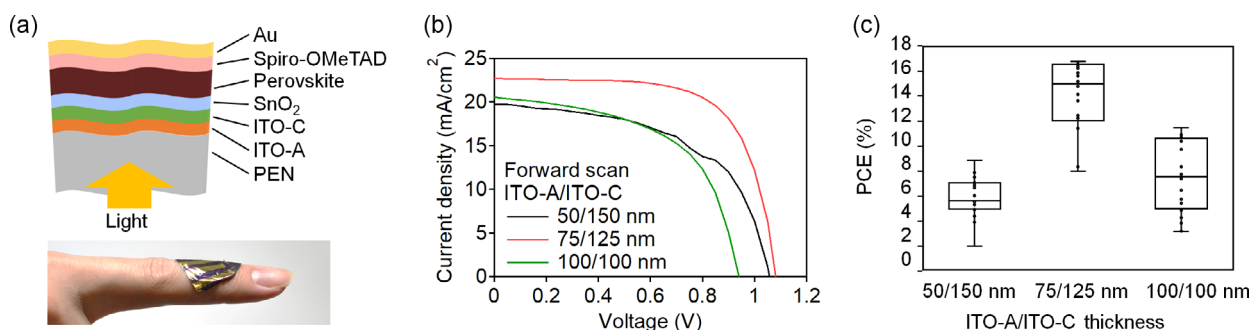

Figure 4. Characteristics of ultrathin perovskite solar cells. a) Device structure of ultrathin perovskite solar cells. b) Current–voltage (J–V) curves of the best-performing cells at 1 sun irradiation. Forward and reverse scans are shown in Figure S9, Supporting Information. c) Box plot showing the PCE for three different ITO-A/ITO-C bilayers, each having a total thickness of 200 nm. More than 18 measurements were made for each bilayer system.
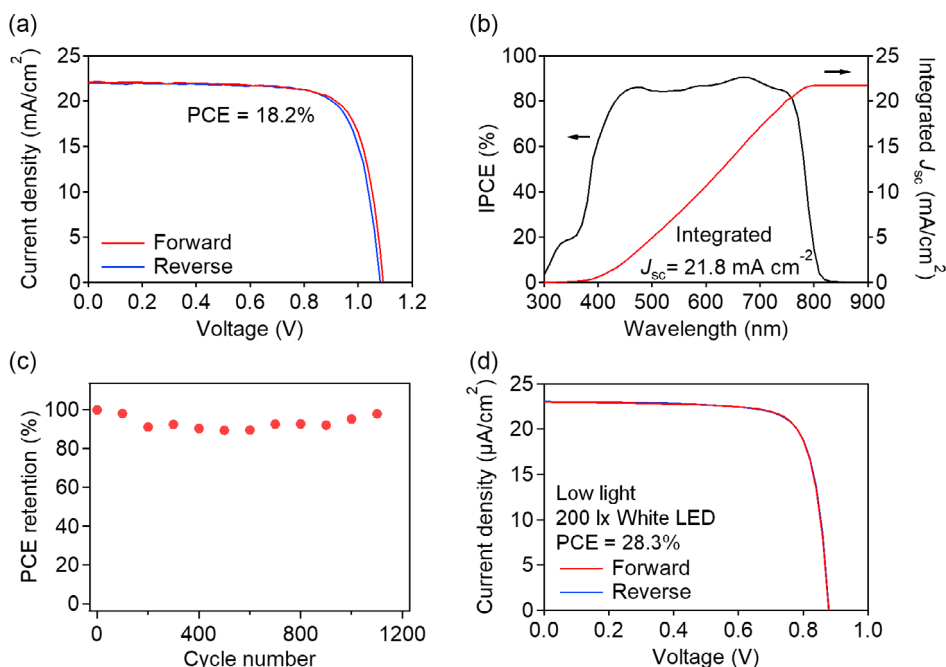
Figure 5. Characterization of the optimized ultrathin perovskite solar cells prepared with 75/125 nm ITO-A/ITO-C bilayers. a) J–V curves measured under 1 sun (AM1.5G), b) incident photon-to-current conversion efficiency (IPCE), and c) bending test with a bending radius of 1 mm, and d) indoor light J–V curves recorded at 200 lx using a white LED.

The ultrathin devices were exceptionally robust toward bending. This may be understood from the mechanics of the bending relation, which inform us that for any given bend radius, a reduction in substrate thickness will reduce the internal stress generated on bending.[40] As shown in Figure 5c, 95% of the initial PCE is retained after 1000 bend cycles (1 mm radius) in ambient air (30% relative humidity). The polycrystalline perovskite layers on the ultrathin film have superior mechanical durability than comparable solar cells fabricated on thick films.[41,42]

Performance under low-intensity light is an important consideration given the potential of ultrathin solar cells to power wearable and internet-of-things devices.[43,44] As shown in Figure 5d, the optimized perovskite solar cells fabricated with 75/125 nm ITO-A/ITO-C bilayers generated 15.8 μW cm^{-2} under a 200 lx

white LED (5000 K), resulting in a nominal PCE under indoor light of 28.3%. Hysteresis remained negligible. The average J_{sc}, V_{oc}, and FF from the forward and reverse J–V scans reached 23.0 μA cm^{-2}, 0.88 V, and 0.79, respectively. Solar cell performance under low-intensity light is often dominated by leakage currents through the perovskite layer.[45] The low-intensity light performance of the ultrathin devices was notably superior to previous reports for flexible perovskite solar cells, mainly because of the high FF, confirming our devices have exceptionally low leakage current.[43,46]

To demonstrate that these ITO bilayer films are also suitable for practical applications, we prepared a 2.3 cm^2 module patterned as three series-connected cells. The module structure is shown in **Figure 6**a and the module is also pictured in the inset
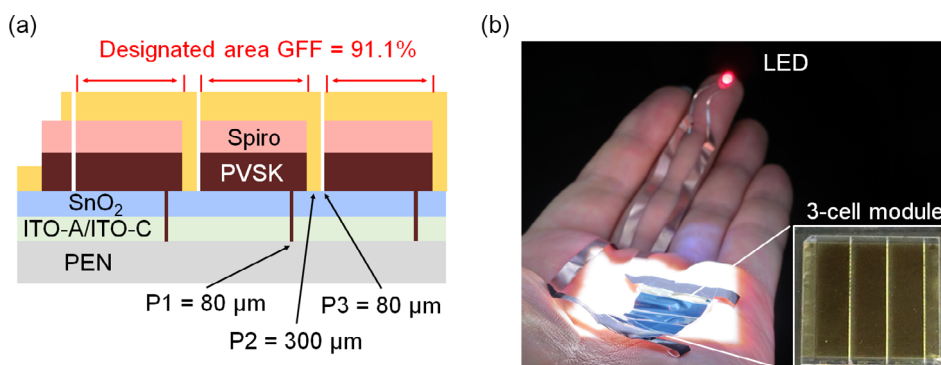

Figure 6. A 3-cell ultrathin perovskite module with a 75/125 nm ITO bilayer patterned using laser scribing. a) The device structure, indicating the designated area and the P1, P2, and P3 scribe lines. b) Photograph of the freestanding ultrathin perovskite module powering a small signal LED. Inset: The finished module before removal from the glass backing plate.

of Figure 6b. Laser scribing is critical for successfully fabricating perovskite solar cell modules on ultrathin films, as mechanical scribing would easily damage the devices. Even with laser scribing, the laser energy must be kept low to avoid damaging the module. Thermal energy transfer to the substrate was kept to a minimum by controlling the pulse duration and spot size. We used a picosecond laser to scribe patterns into the ITO layer (P1, width 80 μm), perovskite/spiro-OMeTAD layers (P2, width 300 μm), and perovskite/spiro-OMeTAD/Au layers (P3, width 80 μm). This fine pattering resulted in a high geometric fill factor of 91.1%. The cell structure was identical to the optimized single-cell devices. From the current–voltage (I–V) curves under AM1.5G shown in Figure S15, Supporting Information, the I_{sc} of the module was 16.5 mA, with $V_{oc} = 3.17$ V (1.06 V cell^{-1}), and FF $= 0.54$. The PCE and maximum power were 12.3% and 28.1 mW, respectively. The open-circuit voltage per cell is comparable to the V_{oc} of the single-cell devices, indicating that recombination losses in the module remain low despite its more complex fabrication. The high V_{oc} is a clear advantage for driving small electronic devices. As pictured in Figure 6b, the freestanding module is operational and capable of driving a small LED.

3. Conclusion

We have demonstrated that smooth, deformation-free ITO layers can be effectively fabricated on ultrathin PEN films by combining thin films of crystalline and amorphous ITO in a bilayer structure. Although amorphous ITO is of limited value as a transparent conducting oxide due to its low electrical conductivity, the positive internal stress was found to effectively balance the negative internal stress of crystalline ITO, resulting in ITO bilayers with low levels of total internal stress. ITO bilayers with a 75 nm amorphous layer and a 125 nm crystalline layer were found to be optimal for solar cell applications, with a sheet resistance of $33 \, \Omega \, \text{sq}^{-1}$ and an average optical transmittance between 400 and 800 nm of 82%.

The deformation-free ITO films were successfully used to fabricate ultrathin and highly flexible perovskite solar cells. Under simulated sunlight, the PCE of the optimized ultrathin solar cells reached 18.2%, with J_{sc} of 22.0 mA cm^{-2}, V_{oc} of 1.09 V, and an FF of 0.76. The devices were physically robust, retaining 95% of the original PCE after 1000 bend cycles. These devices are stable for over 1 year under an inert atmosphere. Under a white LED with an illuminance of 200 lx to simulate indoor lighting conditions, the PCE and FF were 28.3% and 0.79, a promising result showing the strong potential of these cells for energy harvesting applications. 3-cell ultrathin modules with a designated area of 2.3 cm^2 were realized using laser scribing through careful control of the pulse energies. The output under AM1.5G was 28 mW, with a corresponding V_{oc} of 3.17 V. The freestanding module successfully powered a small LED.

The realization of deformation-free sputtered ITO on ultrathin plastic films is an important technological advance, both for the development of ultrathin perovskite solar cells and ultrathin flexible electronic devices in general.

Supporting Information

Supporting Information is available from the Wiley Online Library or from the author.

Conflict of Interest

A.W. is co-founder and CSO of Enecoat Technologies Co., Ltd.

Author Contributions

N.O. and A.W. conceived the idea; N.O., R.K., C.S., and K.Y. fabricated devices and analyzed the data; Y.W. and S.H. performed spectral ellipsometry measurements; H.T., T.H., and Y.K. analyzed spectral data; N.O., T.N., R.M., and A.W. prepared the manuscript. All authors commented on the manuscript. A.W. supervised the work.

Data Availability Statement

The data that support the findings of this study are available from the corresponding author upon reasonable request.

[1] M. Saliba, J. P. Correa-Baena, C. M. Wolff, M. Stolterfoht, N. Phung, S. Albrecht, D. Neher, A. Abate, *Chem. Mater.* **2018**, *30*, 4193.

[2] a) M. A. Green, E. D. Dunlop, G. Siefer, M. Yoshita, N. Kopidakis, K. Bothe, X. Hao, *Prog. Photovoltaics Res. Appl.* **2023**, *31*, 3; b) NREL, https://www.nrel.gov/pv/cell-efficiency.html (accessed: March 2023).

[3] M. Kim, J. Jeong, H. Lu, T. K. Lee, F. T. Eickemeyer, Y. Liu, I. W. Choi, S. J. Choi, Y. Jo, H. B. Kim, S. I. Mo, Y. K. Kim, H. Lee, N. G. An,

京都大学
KYOTO UNIVERSITY

ADVANCED
SCIENCE NEWS

www.advancedsciencenews.com

A Self-archived copy in
Kyoto University Research Information Repository
https://repository.kulib.kyoto-u.ac.jp

京都大学学術情報リポジトリ
KURENAI 紅
Kyoto University Research Information Repository

Solar
www.solar-rrl.com

S. Cho, W. R. Tress, S. M. Zakeeruddin, A. Hagfeldt, J. Y. Kim, M. Grätzel, D. S. Kim, *Science* **2022**, *375*, 302.

[4] A. Al-Ashouri, E. Köhnen, B. Li, A. Magomedov, H. Hempel, P. Caprioglio, J. A. Márquez, A. B. M. Vilches, E. Kasparavicius, J. A. Smith, N. Phung, D. Menzel, M. Grischek, L. Kegelmann, D. Skroblin, C. Gollwitzer, T. Malinauskas, M. Jošt, G. Matic, B. Rech, R. Schlatmann, M. Topic, L. Korte, A. Abate, B. Stannowski, D. Neher, M. Stolterfoht, T. Unold, V. Getautis, S. Albrecht, *Science* **2020**, *370*, 1300.

[5] Y. Hu, T. Niu, Y. Liu, Y. Zhou, C. Xia, C. Ran, Z. Wu, L. Song, P. Müller-Buschbaum, Y. Chen, W. Huang, *ACS Energy Lett.* **2021**, *6*, 2917.

[6] A. Roy, A. Ghosh, S. Bhandari, S. Sundaram, T. K. Mallick, *Buildings* **2020**, *10*, 129.

[7] J. Yoon, U. Kim, Y. Yoo, J. Byeon, S. K. Lee, J. S. Nam, K. Kim, Q. Zhang, E. I. Kauppinen, S. Maruyama, P. Lee, I. Jeon, *Adv. Sci.* **2021**, *8*, 2004092.

[8] S. Park, S. W. Heo, W. Lee, D. Inoue, Z. Jiang, K. Yu, H. Jinno, D. Hashizume, M. Sekino, T. Yokota, K. Fukuda, K. Tajima, T. Someya, *Nature* **2018**, *561*, 516.

[9] M. Kaltenbrunner, M. S. White, E. D. Głowacki, T. Sekitani, T. Someya, N. S. Sariciftci, S. Bauer, *Nat. Commun.* **2012**, *3*, 770.

[10] Z. Jiang, F. Wang, K. Fukuda, A. Karki, W. Huang, K. Yu, T. Yokota, K. Tajima, T. Q. Nguyen, T. Someya, *Proc. Natl. Acad. Sci. U.S.A.* **2020**, *117*, 6391.

[11] H. Zhang, J. Cheng, D. Li, F. Lin, J. Mao, C. Liang, A. K. Y. Jen, M. Grätzel, W. C. H. Choy, *Adv. Mater.* **2017**, *29*, 1604695.

[12] G. Lee, M. C. Kim, Y. W. Choi, N. Ahn, J. Jang, J. Yoon, S. M. Kim, J. G. Lee, D. Kang, H. S. Jung, M. Choi, *Energy Environ. Sci.* **2019**, *12*, 3182.

[13] J. Wu, P. Chen, H. Xu, M. Yu, L. Li, H. Yan, Y. Huangfu, Y. Xiao, X. Yang, L. Zhao, W. Wang, Q. Gong, R. Zhu, *Sci. China Mater.* **2022**, *65*, 2319.

[14] S. Kang, J. Jeong, S. Cho, Y. J. Yoon, S. Park, S. Lim, J. Y. Kim, H. Ko, *J. Mater. Chem. A* **2019**, *7*, 1107.

[15] M. Kaltenbrunner, G. Adam, E. D. Głowacki, M. Drack, R. Schwödiauer, L. Leonat, D. H. Apaydin, H. Groiss, M. C. Scharber, M. S. White, N. S. Sariciftci, S. Bauer, *Nat. Mater.* **2015**, *14*, 1032.

[16] P. Tockhorn, J. Sutter, A. Cruz, P. Wagner, K. Jäger, D. Yoo, F. Lang, M. Grischek, B. Li, J. Li, O. Shargaieva, E. Unger, A. Al-Ashouri, E. Köhnen, M. Stolterfoht, D. Neher, R. Schlatmann, B. Rech, B. Stannowski, S. Albrecht, C. Becker, *Nat. Nanotechnol.* **2022**, *17*, 1214.

[17] B. J. Kim, S. H. Han, J. S. Park, *Thin Solid Films* **2014**, *572*, 68.

[18] A. Wakamiya, N. Ohashi, (Kyoto Univ.), *JP 2022181466A*, **2022**. Priority to JP P2021088419.

[19] U. Kim, M. Han, J. Jang, J. Shin, M. Park, J. Byeon, M. Choi, *Adv. Energy Mater.* **2023**, *13*, 2203198.

[20] H. Kim, C. M. Gilmore, A. Piqué, J. S. Horwitz, H. Mattoussi, H. Murata, Z. H. Kafafi, D. B. Chrisey, *J. Appl. Phys.* **1999**, *86*, 6451.

[21] J. A. Thornton, *J. Vac. Sci. Technol.* **1974**, *11*, 666.

[22] J. A. Thornton, *Annu. Rev. Mater. Sci.* **1977**, *7*, 239.

[23] J. A. Thornton, D. W. Hoffman, *Thin Solid Films* **1989**, *171*, 5.

[24] J. A. Thornton, D. W. Hoffman, *J. Vac. Sci. Technol.* **1977**, *14*, 164.

[25] T. Sasabayashi, N. Ito, E. Nishimura, M. Kon, P. K. Song, K. Utsumi, A. Kaijo, Y. Shigesato, *Thin Solid Films* **2003**, *445*, 219.

[26] G. G. Stoney, *Proc. R. Soc. London, Ser. A* **1909**, *82*, 172.

[27] P. A. Flinn, D. S. Gardner, W. D. Nix, *IEEE Trans. Electron Devices* **1987**, *34*, 689.

[28] R. Ali, M. Sebastiani, E. Bemporad, *Mater. Des.* **2015**, *75*, 47.

[29] Y. Pauleau, *Vacuum* **2001**, *61*, 175.

[30] SCHOTT, https://www.schott.com/en-us/products/d-263-p1000318/technical-details (accessed: March 2023).

[31] J. A. Diaz, R. J. Moon, J. P. Youngblood, *ACS Appl. Mater. Interfaces* **2014**, *6*, 4856.

[32] D. Bhattacharyya, M. J. Carter, *Thin Solid Films* **1996**, *288*, 176.

[33] D. G. Neerinck, T. J. Vink, *Thin Solid Films* **1996**, *278*, 12.

[34] Ossila Ltd., https://www.ossila.com/products/pedot-pss (accessed: March 2023).

[35] M. Ozaki, Y. Ishikura, M. A. Truong, J. Liu, I. Okada, T. Tanabe, S. Sekimoto, T. Ohtsuki, Y. Murata, R. Murdey, A. Wakamiya, *J. Mater. Chem. A* **2019**, *7*, 16947.

[36] H. Tan, A. Jain, O. Voznyy, X. Lan, F. P. G. De Arquer, J. Z. Fan, R. Quintero-Bermudez, M. Yuan, B. Zhang, Y. Zhao, F. Fan, P. Li, L. N. Quan, Y. Zhao, Z. H. Lu, Z. Yang, S. Hoogland, E. H. Sargent, *Science* **2017**, *355*, 722.

[37] W. Gong, H. Guo, H. Zhang, J. Yang, H. Chen, L. Wang, F. Hao, X. Niu, *J. Mater. Chem. C* **2020**, *8*, 11638.

[38] J. Liang, Z. Chen, G. Yang, H. Wang, F. Ye, C. Tao, G. Fang, *ACS Appl. Mater. Interfaces* **2019**, *11*, 23152.

[39] S. Zhang, H. Gu, S. C. Chen, Q. Zheng, *J. Mater. Chem. C* **2021**, *9*, 4240.

[40] M. S. White, M. Kaltenbrunner, E. D. Głowacki, K. Gutnichenko, G. Kettlgruber, I. Graz, S. Aazou, C. Ulbricht, D. A. M. Egbe, M. C. Miron, Z. Major, M. C. Scharber, T. Sekitani, T. Someya, S. Bauer, N. S. Sariciftci, *Nat. Photonics* **2013**, *7*, 811.

[41] S.-K. Lu, J.-T. Huang, J.-H. Lee, J.-J. Wang, D.-S. Liu, *Smart Sci.* **2014**, *2*, 7.

[42] T. Singh, M. Ikegami, T. Miyasaka, *ACS Appl. Energy Mater.* **2018**, *1*, 6741.

[43] S. Kim, H. Oh, G. Kang, I. K. Han, I. Jeong, M. Park, *ACS Appl. Energy Mater.* **2020**, *3*, 6995.

[44] X. He, J. Chen, X. Ren, L. Zhang, Y. Liu, J. Feng, J. Fang, K. Zhao, S. Liu, *Adv. Mater.* **2021**, *33*, 2100770.

[45] M. H. Ann, J. Kim, M. Kim, G. Alosaimi, D. Kim, N. Y. Ha, J. Seidel, N. Park, J. S. Yun, J. H. Kim, *Nano Energy* **2020**, *68*, 104321.

[46] C. Polyzoidis, K. Rogdakis, E. Kymakis, *Adv. Energy Mater.* **2021**, *11*, 2101854.